EISSN: 2231-0916 doi: 10.14202/vetworld.2026.5088-5110 OPEN ACCESS

Veterinary World

RESEARCH ARTICLE

In vitro evaluation of anti-dengue activity of *Zingiber officinale* extract against four dengue virus serotypes: LC-HRMS metabolomic profiling and NS2B-NS3 protease interaction analysis

Mochammad Aqilah Herdiansyah[1], Win Darmanto[2,3], Dwi Winarni[2,3], Ruey-an Doong[4], Putri Ayu Ika Setiyowati[1,5], Aulia Umi Rohmatika[6], Rr Aulia Rahmawati Kusuma Putri[1], Raden Joko Kuncoroningrat Susilo[7], Teguh Hari Sucipto[8] and Putu Angga Wiradana[9]

1. Doctoral Program of Mathematics and Natural Sciences, Faculty of Science and Technology, Universitas Airlangga, Surabaya, Indonesia.
2. Department of Biology, Faculty of Science and Technology, Universitas Airlangga, Surabaya 60115, Indonesia.
3. Research Group Developmental Biology & Biomedical Science, Universitas Airlangga Surabaya 60115, Indonesia.
4. Institute of Analytical and Environmental Sciences, National Tsing Hua University, Sec. 2 Kuang Fu Road, Hsinchu 30013, Taiwan.
5. Study Program of Biology, Faculty of Science and Technology, Universitas Muhammadiyah Lamongan, Lamongan, 62218, Indonesia.
6. Faculty of Medicine, Universitas Pembangunan Nasional Veteran Jawa Timur, Surabaya 60293, Indonesia.
7. Nanotechnology Engineering, Faculty of Advanced Technology and Multidiscipline, Universitas Airlangga, Surabaya 60115, Indonesia.
8. Dengue Study Group, Institute of Tropical Disease, Universitas Airlangga, Surabaya, Indonesia.
9. Study Program of Biology, Faculty of Health and Science, Universitas Dhyana Pura, Bali, Indonesia.

ABSTRACT

Background and Aim: Dengue virus (DENV) infection remains a major public health concern because of its four antigenically distinct serotypes and the limited availability of specific antiviral treatments. *Zingiber officinale* contains diverse phytochemicals with potential antiviral properties; however, its activity against all four DENV serotypes remains insufficiently investigated. This study evaluated the *in vitro* antiviral activity and cytotoxicity of *Z. officinale* ethanolic extract and characterized its metabolites and predicted interactions with DENV NS2B-NS3 proteases.

Materials and Methods: Ginger rhizomes were extracted using 96% ethanol and subjected to liquid chromatography–high-resolution mass spectrometry (LC-HRMS) for metabolite profiling. Putatively annotated metabolites were evaluated using antiviral activity prediction, drug-likeness screening, molecular docking, protein flexibility analysis, and computational pharmacokinetic and toxicity assessment. Extract cytotoxicity was assessed using the MTT assay, whereas antiviral-associated activity against DENV-1–4 was evaluated in Vero E6 cells using a luminescence-based cytopathic effect assay. Experiments were conducted in technical triplicates within a single independent experimental run.

Results: LC-HRMS analysis yielded 45 putatively annotated metabolites. Among the computationally evaluated compounds, 10-deoxymethynolide showed predicted binding affinities of −6.8, −6.5, −6.6, and −7.2 kcal/mol against DENV-1, DENV-2, DENV-3, and DENV-4 NS2B-NS3 proteases, respectively. These predicted interactions require further validation, as the metabolite identity was not confirmed using an authentic analytical standard. The DENV-4 complex exhibited the lowest root mean square fluctuation (1.789 Å). The extract demonstrated concentration-dependent cytotoxicity, with a 50% cytotoxic concentration of 359.93 µg/mL. Cytopathic effects (CPE) decreased across all four serotypes, with estimated 50% effective concentrations of 479.03, 452.87, 425.16, and 419.78 µg/mL, respectively. Corresponding selectivity indices ranged from 0.75 to 0.85, indicating an unfavorable selectivity profile. Notably, all estimated EC_{50} values exceeded the highest experimentally tested concentration of 100 µg/mL, indicating that these estimates were extrapolated beyond the tested concentration range.

Conclusion: *Z. officinale* ethanolic extract was associated with measurable changes in dengue-associated CPE across the four serotypes. However, its low selectivity indices and extrapolated EC_{50} estimates do not support confirmed pan-serotype antiviral efficacy. Computational analysis identified 10-deoxymethynolide as a potential compound for further investigation,

Corresponding Author: Win Darmanto
E-mail: windarmanto@fst.unair.ac.id

Received: 06-07-2026, **Accepted:** 16-10-2026, **Published online:** 10-11-2026

Co-authors: MAH: moch.aqilah.herdiansyah-2024@fst.unair.ac.id; DW: dwi-w@fst.unair.ac.id; RD: radoong@mx.nthu.edu.tw; PAIS: putri.ayu.ika-2023@fst.unair.ac.id; AUR: aulia_umi.fk@upnjatim.ac.id; RAR KP: rr.aulia.rahmawati-2024@fst.unair.ac.id; RJKS: joko.kuncoroningrat@ftmm.unair.ac.id; THS: teguhharisucipto@staf.unair.ac.id; PAW: angga.wiradana@undhirabali.ac.id

How to cite: Herdiansyah MA, Darmanto W, Winarni D, Doong RA, Setiyowati PAI, Rohmatika AU, *et al. In vitro* evaluation of anti-dengue activity of *Zingiber officinale* extract against four dengue virus serotypes: LC-HRMS metabolomic profiling and NS2B-NS3 protease interaction analysis. Vet World, 2026:19(11): 5088-XX.

Copyright: Herdiansyah *et al*. This article is an open access article distributed under the terms of the Creative Commons Attribution 4.0 International License (https://creativecommons.org/licenses/by/4.0/).

but it did not confirm direct protease inhibition. Bioassay-guided fractionation, independent biological replication, purified-compound testing, and direct viral replication assays are required to establish antiviral efficacy and clarify underlying mechanisms.

Keywords: antiviral activity, cytotoxicity, dengue virus, *in vitro* antiviral assay, LC-HRMS metabolomics, molecular docking, NS2B-NS3 protease, *Zingiber officinale.*

INTRODUCTION

Dengue fever is a major mosquito-borne viral disease caused by dengue virus (DENV), which comprises four antigenically distinct serotypes (DENV-1–4). The disease remains a significant public health concern, particularly in tropical and subtropical regions where environmental conditions favor mosquito-vector proliferation and viral transmission. Infection with one DENV serotype generally induces long-lasting immunity against that serotype but does not provide equivalent protection against the other serotypes. Consequently, secondary infection with a heterologous serotype may increase the risk of severe dengue through immunological mechanisms, including antibody-dependent enhancement (ADE). Despite advances in dengue prevention and clinical management, no specific antiviral therapy is currently approved for routine treatment [1]. The predominant transmission cycle involves humans and *Aedes* mosquitoes; however, sylvatic transmission cycles involving nonhuman primates and forest-associated *Aedes* species have also been documented. These ecological interactions underscore the relevance of dengue to veterinary public health and emphasize the importance of a One Health perspective that considers the interconnected roles of human populations, animal hosts, mosquito vectors, and environmental conditions.

Natural products have attracted increasing scientific interest as potential sources of antiviral compounds because of their structural diversity and wide range of biological activities. Several plant-derived phytochemicals have shown antiviral activity against DENV in experimental studies, suggesting their potential relevance to early-stage antiviral drug discovery [2, 3]. *Zingiber officinale* (ginger) is a medicinal plant containing numerous bioactive constituents, including gingerols, shogaols, paradols, diarylheptanoids, and terpenoids. These compounds have been associated with antioxidant, anti-inflammatory, immunomodulatory, and antiviral properties [4–6]. Certain ginger-derived metabolites have also demonstrated predicted interactions with viral proteins in computational investigations, providing preliminary evidence of their potential relevance to antiviral research [7]. Nevertheless, the biological activity of a crude plant extract depends on its phytochemical composition, constituent concentrations, and possible interactions among compounds. Therefore, the presence of metabolites with predicted antiviral properties does not necessarily establish the antiviral efficacy or selectivity of the complete extract.

Liquid chromatography–high-resolution mass spectrometry (LC-HRMS) is a sensitive analytical technique for characterizing complex phytochemical mixtures and generating putative metabolite annotations based on chromatographic and mass spectral characteristics [8]. Combined with computational screening, LC-HRMS-based metabolomic profiling can help prioritize candidate compounds for further experimental investigation. Molecular docking predicts ligand–protein binding orientations and interaction energies, while molecular dynamics-based approaches provide complementary information on protein flexibility and the behavior of predicted molecular complexes [9]. These computational methods are particularly relevant to DENV nonstructural protein 2B–nonstructural protein 3 (NS2B-NS3) protease, an essential component of viral polyprotein processing. Because the NS2B-NS3 protease contributes to the maturation of viral proteins required for replication, it represents an important molecular target for investigating potential DENV inhibitors [10, 11]. These computational approaches provide preliminary insight into possible molecular interactions but do not establish direct protease inhibition or confirm the antiviral activity of individual compounds.

Although the antiviral properties of *Z. officinale* and its phytochemical constituents have attracted considerable attention, evidence regarding the activity of its crude ethanolic extract against all four DENV serotypes remains insufficiently characterized. In particular, the relationship between the phytochemical composition of ginger extract, its effects on DENV-associated cytopathic changes, and its cytotoxicity toward mammalian cells requires further investigation. Evaluating antiviral-associated activity without simultaneously assessing cytotoxicity may lead to an overestimation of therapeutic potential because reduced cytopathic effects (CPE) can occur at concentrations that also compromise host-cell viability. Accordingly, the selectivity index, calculated from the relationship between cytotoxic and antiviral effective concentrations, is essential for distinguishing potentially selective antiviral activity from nonspecific cellular effects.

Another research gap concerns integrating experimental multiserotype screening with metabolomic

characterization and structure-based computational analysis. Although LC-HRMS can reveal the chemical diversity of ginger extracts, chemical profiling alone cannot establish the contribution of individual putatively annotated metabolites to observed biological effects. Similarly, favorable molecular docking scores or predicted protein flexibility do not demonstrate that a compound inhibits the NS2B-NS3 protease under experimental conditions. Integrating these complementary approaches may nevertheless provide a systematic framework for identifying candidate metabolites, evaluating their predicted interactions across DENV serotypes, and prioritizing compounds for subsequent biological validation. This approach supports exploratory antiviral research within a One Health framework, particularly for vector-borne viral diseases involving interactions among human populations, mosquito vectors, animal hosts, and environmental factors.

Previous studies have investigated plant-derived compounds against DENV through multiserotype antiviral screening, metabolite characterization, and computational approaches. In addition, ginger-derived constituents have been explored as potential inhibitors of dengue viral proteins, including the NS2B-NS3 protease, while recent activity-guided investigations have further characterized the antiviral properties of ginger phytochemicals. Nevertheless, differences in experimental models, viral targets, and assay approaches warrant further investigation. Therefore, this study evaluates ethanolic *Z. officinale* rhizome extract against all four DENV serotypes using Vero E6 cells, combining cytotoxicity assessment, LC-HRMS metabolite annotation, and computational analysis of serotype-specific NS2B-NS3 interactions. This framework provides a preliminary assessment of its biological effects and potential molecular interactions.

This study aimed to evaluate the *in vitro* antiviral-associated activity and cytotoxicity of *Z. officinale* ethanolic extract against all four DENV serotypes (DENV-1–4) using a Vero E6 cell culture model and to characterize its putative phytochemical constituents through LC-HRMS-based metabolomic profiling. Specifically, the study sought to determine the concentration-dependent effects of the extract on mammalian cell viability and DENV-associated CPE, estimate the 50% cytotoxic concentration (CC_{50}) and 50% effective concentration (EC_{50}), and calculate the corresponding selectivity indices to assess the relationship between antiviral-associated activity and cytotoxicity.

In addition, the study aimed to prioritize putatively annotated metabolites using computational predictions of antiviral activity and drug-likeness, investigate their predicted interactions with NS2B-NS3 proteases from all four DENV serotypes through molecular docking, and assess selected protein–ligand complexes using protein flexibility and conformational analyses. Computational pharmacokinetic and toxicity assessments were also performed to provide preliminary information on the characteristics of selected candidate metabolites. The study hypothesized that *Z. officinale* ethanolic extract would produce measurable changes in DENV-associated CPE across multiple serotypes and that selected putative metabolites would exhibit favorable predicted interactions with NS2B-NS3 proteases. By integrating cell-based assays, metabolomic profiling, and computational analyses, the study sought to generate preliminary evidence to guide subsequent investigations of purified phytochemical constituents, antiviral selectivity, and potential mechanisms of action.

MATERIALS AND METHODS

Ethical approval

The study involved *in vitro* experiments using established Vero cell cultures and DENV strains, together with phytochemical and computational analyses. No experiments involving live animals or human participants were described.

Study period and location

The study was conducted from October 2025 to July 2026. Both *in vitro* experiments and *in silico* analyses were performed at the Dengue Laboratory, Institute of Tropical Disease, Universitas Airlangga, Surabaya, Indonesia. Fresh *Z. officinale* rhizomes were collected on February 19, 2026, from Tanjung Market, Mojokerto City, East Java, Indonesia (7°28′1″S, 112°26′12″E). The Vero E6 cell cultures and DENV strains were obtained from the Institute of Tropical Diseases, Universitas Airlangga, Surabaya, Indonesia.

Study design

The study integrated phytochemical profiling, *in silico* screening, and *in vitro* evaluation of *Z. officinale* ethanolic extract. LC-HRMS was used for metabolite profiling. The putatively annotated metabolites were screened for drug-likeness and predicted antiviral activity, followed by molecular docking, protein flexibility analysis, conformational assessment, and pharmacokinetic and toxicity predictions. The *in vitro* component

evaluated the cytotoxicity of the extract and its effects on DENV-associated cytopathic changes using Vero cell cultures. All four DENV serotypes (DENV-1–4) were included in the antiviral assay.

Sample collection and preparation of extract

Fresh *Z. officinale* rhizomes weighing 1 kg were collected and air-dried at room temperature (24–29°C) for approximately 7 days until completely dry, yielding approximately 350 g of dried material. The dried rhizomes were subsequently subjected to ethanolic extraction. The botanical identity of the plant material was confirmed based on morphological characteristics following standard taxonomic criteria. A voucher specimen was deposited in the Department of Biology, Universitas Airlangga, under voucher number 05/09.ZO/2026.

The dried rhizomes were extracted using 96% ethanol (Sumber Ilmiah Persada, Surabaya, Indonesia) at a ratio of 1:3 (w/v). Extraction was performed in three consecutive cycles, using 1050 mL of ethanol per cycle. After each cycle, the solvent was separated and replaced with fresh ethanol. Each extraction cycle was performed for 3 days (72 hours). All extraction cycles were performed under the same conditions for a predetermined duration. A single batch of *Z. officinale* ethanolic extract was used throughout the study. The chemical composition of the extract was characterized using LC-HRMS, and the detected metabolites were reported as putative annotations. Quantitative standardization using specific chemical marker compounds was not performed.

The combined extracts were concentrated using a rotary evaporator (IKA-Werke GmbH & Co. KG, Staufen, Germany) at 40–60°C, a rotation speed of 80–120 rpm, and a vacuum pressure of 100–200 mbar. The concentrated extract was collected and transferred into vials for subsequent analyses. The final extract weighed 60 g, corresponding to a 6% extraction yield based on the initial fresh plant material and approximately 17.1% based on the dried rhizome weight. The extract was stored at 4°C until further use.

LC-HRMS analysis

The ginger extract was mixed with methanol and filtered through a 0.2-µm nylon membrane (Millex™, Merck KGaA, Darmstadt, Germany) before analysis. Metabolite profiling was performed using a Vanquish ultra-high-performance liquid chromatography system coupled to a Q Exactive Plus Orbitrap high-resolution mass spectrometer (Thermo Fisher Scientific, Massachusetts, USA), equipped with an Accucore™ C18 column (Thermo Fisher Scientific). The mobile phases consisted of water containing 0.1% formic acid (A) and acetonitrile containing 0.1% formic acid (B). The gradient program was as follows: 5% B (0-1 min), 5-95% B (1-25 min), 95% B (25-28 min), and 5% B (28-33 min).

The analytical conditions included a column temperature of 30°C, an injection volume of 2 µL, a flow rate of 0.2 mL/min, and a mass-to-charge ratio (*m/z*) range of 100–1500. Analyses were performed in both positive and negative ionization modes.

The acquired data were processed using Compound Discoverer version 3.2 (Thermo Fisher Scientific Inc., Waltham, Massachusetts, USA) with the mzCloud (https://www.mzcloud.org) mass spectral library and ChemSpider chemical database (https://www.chemspider.com). Metabolites were reported as putative annotations based on accurate-mass measurements and available library information rather than definitive compound identifications.

***In silico* study**

Tabulation of phytochemical compounds based on LC-HRMS results: The LC-HRMS screening results were tabulated by arranging the putatively annotated compounds in descending order of chromatographic peak area percentage. Higher peak area percentages indicated greater relative signal abundance within the analyzed sample rather than higher absolute metabolite concentrations.

Information on each compound, including its molecular formula, compound identification number (CID), canonical simplified molecular-input line-entry system (SMILES) notation, and three-dimensional (3D) structure, was retrieved from the PubChem database (https://pubchem.ncbi.nlm.nih.gov/). Quercetin (CID: 5280343) was used as the positive control for the computational analysis.

Screening of drug-likeness and predicted antiviral activity: Drug-likeness screening of the putatively annotated metabolites was performed using the SCFBio web server (https://scfbio-iitd.res.in/software/drugdesign/lipinski.jsp). The assessment was based on Lipinski's Rule of Five (Ro5), using the following criteria: molecular weight ≤500 Da, logarithm of the octanol–water partition coefficient (logP) ≤5, hydrogen bond donors ≤5, hydrogen bond acceptors ≤10, and molar refractivity of 40–130 [12].

Compounds meeting the Ro5 screening criteria were subsequently evaluated using the PASS Online web server (https://way2drug.com/PassOnline/) to predict their potential anti-dengue or anti-flavivirus activity. The

predictions were expressed as the probability of activity (Pa) and probability of inactivity (Pi). Compounds with Pa > Pi were considered to have predicted antiviral potential.

The three compounds with the highest Pa values were selected for molecular docking against the nonstructural protein targets of the four DENV serotypes.

Preparation of NS2B-NS3 protein receptors: The three-dimensional structures of DENV nonstructural protein 2B–nonstructural protein 3 (NS2B-NS3) proteases were retrieved from the Protein Data Bank (PDB; https://www.rcsb.org/). The NS2B-NS3 protease was selected as the molecular target because of its role in viral polyprotein processing, its conserved catalytic region, and the availability of experimentally determined structures representing all four DENV serotypes [11].

The catalytic triad comprising histidine, aspartate, and serine (His–Asp–Ser), together with the conserved S1, S2, and S3 binding pockets, provides a structural basis for comparative docking across DENV serotypes [10].

The receptor structures used were DENV-1 (PDB ID: 3L6P), DENV-2 (PDB ID: 2FOM), DENV-3 (PDB ID: 3U1I), and DENV-4 (PDB ID: 2VBC) (Table 1).

Before molecular docking, water molecules and associated ligands were removed from the receptor structures using PyMOL version 1.74 (Schrödinger, LLC, USA) [13].

Table 1: Protein structures and docking grid parameters for NS2B-NS3 proteases of four dengue virus serotypes.

Serotype	Protein	Domain	PDB ID	Grid center X	Grid center Y	Grid center Z	Grid size X	Grid size Y	Grid size Z	Information
DENV-1	NS2B-NS3	Protease	3L6P	−21.418	−17.354	25.252	59.813	78.371	52.237	Active structure, widely used
DENV-2	NS2B-NS3	Protease	2FOM	0.372	−17.155	13.947	65.023	64.458	43.862	Classical reference structure
DENV-3	NS2B-NS3	Protease	3U1I	35.184	−25.959	27.143	91.668	101.520	67.501	Good resolution
DENV-4	NS2B-NS3	Protease	2VBC	−6.069	2.851	20.867	96.398	65.233	100.268	Valid and active structure

DENV = Dengue virus; NS2B-NS3 = Nonstructural protein 2B–nonstructural protein 3 protease; PDB = Protein Data Bank; RMSD = Root mean square deviation. Grid center coordinates and dimensions are expressed in Å. — = Not reported.

Molecular docking: Molecular docking was performed using the AutoDock Vina algorithm implemented in PyRx version 0.8 (SourceForge, San Diego, CA, USA). The docking parameters included an exhaustiveness value of 8 and a maximum of nine binding modes.

Predicted ligand–receptor binding affinities were expressed in kcal/mol. For each ligand–receptor combination, the docking pose with the most favorable predicted binding affinity was selected for subsequent interaction analysis. More negative docking scores were interpreted as indicating more favorable predicted ligand–receptor interactions within the docking model [14, 15].

Molecular dynamics-based protein flexibility analysis: The molecular docking results were further evaluated using the CABS-flex 3.0 web server (https://lcbio.pl/cabsflex3/) to assess the predicted flexibility of the selected protein structures [16].

The best-scoring docking pose for each receptor–ligand complex was selected as the input model. The analysis was performed using the server's default settings, and the resulting root mean square fluctuation (RMSF) profiles were used to assess predicted residue-level flexibility [17].

Simulation parameters, including the number of cycles and replicate settings, followed the default configuration provided by the CABS-flex 3.0 server.

Conformational analysis of NS2B-NS3 proteins using Ramachandran plots: The conformational characteristics of the NS2B-NS3 protein structures from the four DENV serotypes were evaluated using Ramachandran plots generated through the RamPlot web server (https://ramplot.in/).

Protein structures in PDB format were uploaded to the server, and the distributions of the backbone dihedral angles phi (ϕ) and psi (ψ) were examined for individual amino acid residues [18].

Prediction of pharmacokinetic properties and toxicity: The absorption, distribution, metabolism, and excretion (ADME) properties of the selected compounds were predicted using the pkCSM web server (https://biosig.lab.uq.edu.au/pkcsm/).

Canonical SMILES representations were submitted to the server to estimate pharmacokinetic properties across the corresponding ADME parameters [19, 20].

Predicted toxicity profiles were subsequently evaluated using the ProTox 3.0 web server (https://tox.charite.de/protox3/) [21].

In vitro study

Cytotoxicity assay of ginger extract: The cytotoxicity of *Z. officinale* ethanolic extract was evaluated using the 3-(4,5-dimethylthiazol-2-yl)-2,5-diphenyltetrazolium bromide (MTT) assay.

Vero E6 cells were seeded into 96-well plates at a density of 5×10^4 cells/mL and treated with ginger extract at concentrations of 31.25, 62.5, 125, 250, 500, and 1000 µg/mL. Each concentration was tested in triplicate.

The treated cells were incubated for 4 days at 37°C in an atmosphere containing 5% CO_2. Subsequently, 15 µL of MTT solution (Promega, Madison, WI, USA) was added to each well, and the plates were incubated for an additional 4 h at 37°C.

Following incubation, 100 µL of stop solution was added to each well. Optical density (OD) was measured at 570 nm.

Preparation of Vero E6 cells and DENV cultures*:* Vero E6 cells (American Type Culture Collection CRL-1586; Merck, USA) were obtained from the Institute of Tropical Diseases, Universitas Airlangga, Indonesia.

The cells were maintained in Dulbecco's modified Eagle medium (DMEM; Merck, USA) supplemented with 10% fetal bovine serum (FBS; Merck, USA) and 1% penicillin–streptomycin. Cultures were incubated at 37°C in a humidified atmosphere containing 5% CO_2.

The DENV strains used in this study were DENV-1 (isolate code: AB915377), DENV-2 (isolate code: KT012509), DENV-3 (isolate code: KF709426), and DENV-4 (isolate code: KT204464). All viral strains were at passage 66 and were provided by the Dengue Laboratory, Institute of Tropical Diseases, Universitas Airlangga, Indonesia.

Viral stocks were quantified using a focus-forming unit (FFU) assay and standardized to an infectious titer of 2×10^3 FFU/mL for the antiviral assay. Before the cell-based assays, 1 g of the concentrated extract was reconstituted in ethanol. The resulting solution was subsequently diluted with DMEM to obtain the required treatment concentrations. Ethanol without extract was used as the vehicle control.

Evaluation of anti-dengue activity: The antiviral-associated activity of *Z. officinale* ethanolic extract was evaluated using the Viral ToxGlo™ assay (Promega, Madison, WI, USA), which measures luminescence associated with cellular viability and virus-induced CPE.

The assay was performed using 96-well flat-bottom luminescence microplates. Before treatment, the culture medium was removed from the wells. Minimum essential medium (MEM; Merck KGaA, Darmstadt, Germany), supplemented with 10% FBS, was added at a volume of 50 µL to the medium-control and cell-control wells and 25 µL to the designated sample wells.

The extract was evaluated at five concentrations: 6.25, 12.5, 25, 50, and 100 µg/mL. Each concentration was tested in triplicate.

Subsequently, 25 µL of DENV stock solution was added to the corresponding sample wells, whereas 50 µL of DENV control was added to the designated control wells.

The microplates were incubated for 48–144 h at 37°C in a humidified atmosphere containing 5% CO_2. Following incubation, 100 µL of Viral ToxGlo™ reagent was added to each well, and the plates were incubated for an additional 10 min at 37°C in 5% CO_2.

Luminescence was measured using a GloMax® microplate reader (Promega Corporation, Madison, WI, USA) [22].

All *in vitro* experiments were performed using three technical replicates (three wells per concentration) within a single independent experiment conducted on the same day. The three wells represented technical replicates rather than independent biological replicates.

Statistical analysis

The 50% cytotoxic concentration (CC_{50}) and 50% effective concentration (EC_{50}) were estimated from concentration–response data using nonlinear regression with a four-parameter logistic (4PL) model.

Concentration–response curves were fitted using nonlinear least-squares regression, and CC_{50} and EC_{50} estimates were obtained from the fitted models together with their corresponding 95% confidence intervals (CIs). EC_{50} values exceeding the highest tested concentration (100 µg/mL) were identified as extrapolated estimates and interpreted cautiously. Statistical analyses were performed using GraphPad Prism version 11.1.0 (GraphPad Software, USA).

The selectivity index (SI) was calculated as the ratio of CC_{50} to EC_{50} using the following equation:

$$SI = CC_{50}/EC_{50}$$

Differences in antiviral-associated activity among the four DENV serotypes were interpreted descriptively without inferential statistical comparisons. Statistical significance was set at $p < 0.05$, where applicable.

RESULTS

Phytochemical profile of *Z. officinale* extract determined by LC-HRMS

The metabolite profile of the *Z. officinale* ethanolic extract was characterized using LC-HRMS (Table 2). A total of 45 compounds were detected in the crude extract, including terpenoids, phenolic compounds, fatty acid derivatives, alkaloids, steroids, and organic acids. The detected metabolites exhibited different retention times and chromatographic peak areas.

Among the putatively annotated compounds, cyclandelate exhibited the highest peak area (15,203,337,878), followed by 20-α-dihydrodydrogesterone (6,878,110,562), α-farnesene (4,642,324,983), and lasiocarpine (4,051,593,569). Other detected compounds included paradol, curcumene, falcarindiol, hexahydrocurcumin, ethyl cinnamate, and 4-methoxycinnamic acid.

Terpenoid-associated compounds represented a prominent group among the detected metabolites, including α-farnesene, kaur-16-ene, steviol, azafrin, and nootkatone.

Table 2: Putatively annotated metabolites detected in *Zingiber officinale* ethanolic extract using LC-HRMS.

No.	Compound	Molecular formula	Molecular weight	Retention time (min)	Delta mass (ppm)	ChemSpider results	mzCloud best match	Sample area
1	Cyclandelate	C17H24O3	276.17	15.34	0.40	11	96.7	15203337878
2	20-α-dihydrodydrogesterone	C21H32O3	332.23	20.93	0.40	21	98.1	6878110562
3	α-farnesene	C15H24	204.19	21.89	1.23	207	98.1	4642324983
4	Lasiocarpine	C21H33NO7	411.23	12.47	3.99	1	98.1	4051593569
5	6-β-hydroxy-testosterone	C19H28O3	304.20	18.21	0.50	28	98.1	3841777937
6	Benzyl formate	C8H8O2	136.05	18.84	1.13	26	73.1	3651623813
7	Choline	C5O13NO	103.10	1.05	4.70	0	96	3416003300
8	9-octadecenamide	C18H35NO	281.27	25.35	0.44	3	94.6	3311430226
9	Ethyl cinnamate	C11H12O2	176.08	15.33	1.28	25	96.1	2463294048
10	Falcarindiol	C17H24O2	260.18	14.76	1.29	7	82.1	2254326266
11	Kaur-16-ene	C20H32	272.25	26.42	0.38	58	60.6	2027003374
12	Hecogenin	C27H42O4	430.31	26.96	0.56	11	60.6	2002328896
13	Algestone acetophenide	C29H36O4	448.26	20.64	−2.98	2	60.6	1494777300
14	Vigabatrin	C6H11NO2	129.08	1.21	2.98	19	98.8	1450547413
15	4-methoxycinnamic acid	C10H10O3	178.06	15.33	0.66	29	83.5	1358682335
16	1-[(3-carboxypropyl)amino]-1-deoxy-β-D-fructofuranose	C10H19NO7	265.12	1.05	0.86	1	83.5	1295806037
17	Octinoxate	C18H26O3	290.19	16.85	1.03	5	83.5	1164759742
18	Dihexyl phthalate	C20H30O4	334.21	21.37	0.26	37	83.5	1150673955
19	Epristeride	C25H37NO3	399.28	24.96	1.13	1	83.5	1123622169
20	Malic acid	C4H6O5	134.02	1.21	−4.06	6	96.9	1082383862
21	Safrole	C10H10O2	162.07	14.75	1.27	32	93.3	1022027823
22	10-deoxymethynolide	C17H28O4	296.20	14.76	0.48	3	93.3	1010772152
23	Myricanone	C21H24O5	356.16	12.09	0.68	31	93.3	986066252
24	Steviol	C20H30O3	318.22	21.25	0.40	58	74.7	949402701
25	2-C-methylerythritol 4-phosphate	C5H13O7P	216.04	1.15	1.39	2	72.3	931696682
26	Curcumene	C15H22	202.17	19.73	1.66	13	72.3	920811893
27	Stacyhydrine	C7H13NO2	143.09	1.106	2.19	7	98.3	863017547
28	Azafrin	C27H38O4	426.28	23.82	0.82	2	98.3	833993694
29	Hexahydrocurcumin	C21H26O6	374.17	12.08	2.04	11	96.9	771794904
30	Delsoline	C25H41NO7	467.29	16.92	3.10	3	68.9	685524376
31	Glucoheptonic acid	C7H14O8	226.07	1.13	0.78	1	98	679721336
32	Muramic acid	C9H17NO7	251.10	1.06	1.31	3	67.1	649818787
33	Bucromarone	C29H37NO4	463.27	21.89	2.66	1	67.1	627227232
34	Paravallarine	C22H33NO2	343.25	22.33	0.94	8	67.1	625663086
35	Acetylmethadol	C23H31NO2	353.23	22.93	0.64	3	67.1	619469901
36	Palmitamide	C16H33NO	255.26	24.86	0.71	1	98.5	617334522
37	Arabic acid	C5H10O6	166.05	1.09	2.08	8	98.5	612072789
38	Picrasin B	C21H28O6	376.19	11.36	2.00	5	98.5	599446068

No.	Compound	Molecular formula	Molecular weight	Retention time (min)	Delta mass (ppm)	ChemSpider results	mzCloud best match	Sample area
39	Paradol	C17H26O3	278.19	14.76	0.75	6	98.5	582367215
40	Linalyl benzoate	C17H22O2	258.16	15.33	1.75	12	64.5	548237192
41	Epi-tulipinolide	C17H22O4	290.15	20.48	0.32	11	72.8	523307169
42	Vitamin A	C20H30O	286.23	27.02	−0.01	27	84	493537863
43	Nootkatone	C15H22O	218.17	22.36	1.42	54	84	492606231
44	Decoquinate	C24H35NO5	417.25	18.35	1.77	3	60.9	486242463

LC-HRMS = Liquid chromatography–high-resolution mass spectrometry; min = Minutes; ppm = Parts per million; MS/MS = Tandem mass spectrometry. Data were acquired in positive and negative electrospray ionization modes. Metabolite identities are putative annotations based on accurate mass and/or MS/MS spectral matching.

Several compounds, including cyclandelate, 20-α-dihydrodydrogesterone, and lasiocarpine, were tentatively annotated through library-based matching. These assignments should be interpreted cautiously because their identities were not confirmed using authentic reference standards or standard-matched retention times. Therefore, they are reported as putative annotations, and their occurrence as genuine phytochemical constituents of *Z. officinale* remains unverified.

Drug-likeness and predicted antiviral potential of putatively annotated metabolites

The predicted antiviral potential of the metabolites annotated by LC-HRMS was evaluated using PASS Online based on the previously defined Pa and Pi parameters (Table 3). Compounds with Pa values exceeding their corresponding Pi values were considered for further screening.

Among the annotated compounds, α-farnesene exhibited the highest predicted antiviral activity (Pa = 0.764), followed by muramic acid (Pa = 0.717) and 10-deoxymethynolide (Pa = 0.688). All three compounds had Pi values below 0.01. Other metabolites, including dihexyl phthalate, curcumene, palmitamide, ethyl cinnamate, and linalyl benzoate, exhibited Pa values ranging from 0.665 to 0.668. In contrast, kaur-16-ene, delsoline, and picrasin B showed lower Pa values accompanied by relatively higher Pi values.

Table 3: Predicted antiviral potential of putatively annotated metabolites.

No.	Compound	CID	Pa	Pi
1	Cyclandelate	2893	0.577	0.015
2	20-α-dihydrodydrogesterone	101787691	0.390	0.050
3	α-farnesene	5362889	0.764	0.002
4	Lasiocarpine	5281735	0.506	0.022
5	6-β-hydroxy-testosterone	65543	0.554	0.017
6	Benzyl formate	7708	0.444	0.079
7	Choline	305	—	—
8	9-octadecenamide	1930	0.657	0.009
9	Ethyl cinnamate	637758	0.665	0.009
10	Falcarindiol	5281148	0.602	0.006
11	Kaur-16-ene	10901750	0.265	0.116
12	Hecogenin	91453	0.362	0.054
13	Algestone acetophenide	5284538	0.435	0.059
14	Vigabatrin	5665	0.571	0.026
15	4-methoxycinnamic acid	699414	0.543	0.034
16	1-[(3-carboxypropyl)amino]-1-deoxy-β-D-fructofuranose	101040890	0.643	0.013
17	Octinoxate	5355130	0.493	0.027
18	Dihexyl phthalate	6786	0.688	0.007
19	Epristeride	68741	0.467	0.028
20	Malic acid	525	0.573	0.009
21	Safrole	5144	0.356	0.050
22	10-deoxymethynolide	5282031	0.688	0.006
23	Myricanone	161748	0.292	0.097
24	Steviol	452967	0.435	0.036
25	2-C-methylerythritol 4-phosphate	443198	0.566	0.010
26	Curcumene	92139	0.688	0.033
27	Stacyhydrine	115244	0.404	0.107
28	Azafrin	5281225	0.592	0.021
29	Hexahydrocurcumin	5318039	0.422	0.070

No.	Compound	CID	Pa	Pi
30	Delsoline	44655937	0.256	0.088
31	Glucoheptonic acid	25588	0.645	0.004
32	Muramic acid	441038	0.717	0.005
33	Bucromarone	132852	0.396	0.096
34	Paravallarine	442980	0.576	0.015
35	Acetylmethadol	10517	0.340	0.060
36	Palmitamide	69421	0.666	0.009
37	Arabic acid	122045	0.645	0.004
38	Picrasin B	12313355	0.338	0.179
39	Paradol	94378	0.415	0.076
40	Linalyl benzoate	31353	0.670	0.003
41	Epi-tulipinolide	5281505	0.481	0.032
42	Vitamin A	445354	0.421	0.027
43	Nootkatone	1268142	0.349	0.061
44	Decoquinate	29112	0.558	0.011

CID = PubChem compound identifier; Pa = Probability of activity; Pi = Probability of inactivity. The three selected compounds for further computational analysis were α-farnesene, muramic acid, and 10-deoxymethynolide. — = Prediction not reported.

The three metabolites with the highest predicted antiviral activity (α-farnesene, muramic acid, and 10-deoxymethynolide) were further evaluated for drug-likeness using Lipinski's Ro5 criteria (Table 4). Most of the evaluated parameters for these compounds were within the ranges specified by the screening criteria.

Among the three metabolites, 10-deoxymethynolide exhibited the most favorable drug-likeness profile, with a molecular weight of 296.40 Da, one hydrogen bond donor, four hydrogen bond acceptors, a logP value of 2.74, and a molar refractivity of 83.89. All these parameters satisfied the applied Lipinski criteria, suggesting favorable predicted drug-likeness characteristics.

Table 4: Drug-likeness assessment of three metabolites selected on the basis of predicted antiviral potential.

Compound	MW (Da)	HBD	HBA	logP	MR
α-farnesene	204.35	0	0	5.20	72.32
Muramic acid	251.23	5	8	−2.76	53.50
10-deoxymethynolide	296.40	1	4	2.74	83.89

MW = Molecular weight; Da = Dalton; HBD = Hydrogen bond donors; HBA = Hydrogen bond acceptors; logP = Logarithm of the octanol–water partition coefficient; MR = Molar refractivity. Screening criteria: MW ≤ 500 Da, HBD ≤ 5, HBA ≤ 10, logP ≤ 5, and MR = 40–130. The logP value of α-farnesene exceeds the specified threshold.

Lipinski's Rule of Five was applied as a preliminary computational screening approach to assess the drug-likeness of the selected compounds based on their physicochemical properties. Compliance with these criteria suggests potentially favorable drug-like characteristics but does not independently confirm oral absorption, bioavailability, or membrane permeability.

Molecular docking analysis of metabolites against NS2B-NS3 proteases

Molecular docking was performed using three selected metabolites, namely α-farnesene, muramic acid, and 10-deoxymethynolide, against the NS2B-NS3 proteins of the four DENV serotypes (Table 5).

Among the tested metabolites, 10-deoxymethynolide exhibited the most favorable predicted binding affinities across all four serotypes, with docking scores of −6.8 kcal/mol for DENV-1, −6.5 kcal/mol for DENV-2, −6.6 kcal/mol for DENV-3, and −7.2 kcal/mol for DENV-4. The positive control, quercetin, exhibited docking scores ranging from −7.6 to −7.8 kcal/mol. In comparison, α-farnesene showed docking scores ranging from −4.7 to −5.8 kcal/mol, whereas those of muramic acid ranged from −5.6 to −6.5 kcal/mol.

The most favorable docking score for 10-deoxymethynolide was observed against the DENV-4 NS2B-NS3 protein (−7.2 kcal/mol). The predicted interaction profile involved Pro543(A), Val544(A), Leu429(A), Arg387(A), Ile365(A), and His487(A).

For DENV-1, 10-deoxymethynolide interacted with Trp17(A), Lys43(A), Gly142(A), and Glu143(A), with additional hydrophobic interactions involving Leu31(A), Ile30(A), and Ile42(A). In the DENV-2 and DENV-3 complexes, the ligand interacted with residues surrounding the corresponding binding pockets.

Conformational dynamics of ligand–NS2B-NS3 complexes

The conformational dynamics of the 10-deoxymethynolide–NS2B-NS3 complexes were evaluated using RMSF analysis across the four DENV serotypes (Figure 2).

Table 5: Predicted molecular docking interactions of selected metabolites and quercetin with NS2B-NS3 proteases from four dengue virus serotypes.

Compound	Receptor	Binding affinity (kcal/mol)	Interaction type	Amino acid residues
α-farnesene	DENV-1 NS2B-NS3	−4.7	vdw	Gln160(A), Asn29(A), Glu144(A), Glu143(A)
			HI	Arg192(A), Trp17(A), Ile30(A), Leu31(A), Lys43(A)
	DENV-2 NS2B-NS3	−5.8	vdw	Val146(B), Gly87(B), Val147(B), Gly148(B), Ile165(B), Asn152(B), Ala166(B), Asn167(B), Lys73(B)
			HI	Ile123(B), Val154(B), Ala164(B), Lys74(B), Leu76(B), Trp83(B), Leu149(B), Leu85(B)
	DENV-3 NS2B-NS3	−4.8	vdw	Thr68(C), Asp129(D), Glu101(D)
			HI	Phe130(D), Leu128(D), Phe109(D), Lys104(D), Lys107(D)
	DENV-4 NS2B-NS3	−5.4	vdw	Asp603(A), Ser386(A), Thr408(A), Asp409(A), Ser364(A), Pro363(A)
			HI	Arg599(A), Ile365(A), Arg387(A), Lys388(A), Leu443(A), Leu429(A), Ala602(A)
Muramic acid	DENV-1 NS2B-NS3	−6.0	vdw	Tyr200(A), Gly203(A), Gly201(A), Asp179(A), His101(A), Lys181(A)
			HI	Pro182(A)
			PHI	Phe180(A), Ser213(A), Asn202(A), Thr184(A), Gly183(A), Ser185(A)
	DENV-2 NS2B-NS3	−5.6	vdw	Ile165(B), Ile164(B), Lys74(B), Asn167(B), Ala166(B), Leu85(B), Gly87(B), Val146(B), Leu149(B), Met49(B), Leu76(B)
			PHI	Trp83(B), Val147(B), Asn152(B)
	DENV-3 NS2B-NS3	−5.8	vdw	Gly151(D), Pro132(D), Val52(D), Tyr150(D), Thr134(D), Val155(D), Asn152(D)
			PHI	Tyr161(D), Lys131(D), Gly133(D), Ser135(D), Gly153(D), Phe130(D), His51(D)
	DENV-4 NS2B-NS3	−6.5	vdw	Phe288(A), Trp488(A), Lys430(A), His485(A), Cys428(A), Leu429(A), Thr317(A), Ala452(A), Thr450(A)
			HI	His287(A)
			PHI	Glu412(A), Thr289(A), Ser453(A), Asp409(A), Asp482(A)
10-deoxymethynolide	DENV-1 NS2B-NS3	−6.8	vdw	Trp17(A), Lys43(A), Asn29(A), Gly142(A), Glu143(A)
			HI	Leu31(A), Ile30(A), Ile42(A)
			PHI	Arg192(A), Glu144(A)
	DENV-2 NS2B-NS3	−6.5	vdw	Val146(B), Leu149(B), Gly148(B), Val147(B), Gly87(B), Glu88(B), Glu86(B)
			HI	Leu76(B), Trp69(B), Leu85(B)
			PHI	Trp83(B), Lys74(B)
	DENV-3 NS2B-NS3	−6.6	vdw	Thr168(B), Gln167(B), Thr120(B), Gly124(B), Gln167(B), Gln88(B), Glu122(B)
			HI	Ile123(B), Ile165(B)
			PHI	Asn169(B), Trp89(B)
	DENV-4 NS2B-NS3	−7.2	vdw	Pro543(A), Val544(A), Pro431(A), Leu429(A), Asp603(A), Ala602(A)
			HI	Arg387(A), Ile365(A), Arg599(A), Pro291(A)
			PHI	His487(A)
Quercetin (control)	DENV-1 NS2B-NS3	−7.8	vdw	Leu178(A), Asp179(A), Tyr200(A), Thr184(A), Val102(A), Gly87(A), Pro182(A), Tyr211(A), Val205(A), Asn202(A)
			PHI	Ser185(A)
			Unfavorable donor–donor	Lys181(A)
	DENV-2 NS2B-NS3	−7.8	vdw	Asn152(B), Met49(B), Ala164(B), Ala166(B), Lys74(B), Trp83(B), Gly148(B), Glu88(B), Gly87(B), Glu86(B)

doi: 10.14202/vetworld.2026.5088-5110

Compound	Receptor	Binding affinity (kcal/mol)	Interaction type	Amino acid residues
			PHI	Leu85(B), Leu149(B)
			π–sigma	Leu76(B)
			Amide–π stacked	Ile165(B)
	DENV-3 NS2B-NS3	−7.6	vdw	Thr83(C), Met84(C), Gly153(D), Gly133(D), Lys131(D), Pro132(D), Tyr161(D)
			PHI	Asp129(D), Phe130(D), Ser135(D), His51(D), Asn152(D)
			π–π T-shaped	Tyr150(D)
			Unfavorable donor–donor	Thr134(D)
	DENV-4 NS2B-NS3	−7.8	vdw	Tyr278(A), Thr252(A), Val257(A), Arg254(A), Glu255(A), Asn277(A), Ser249(A), Arg274(A), Asp258(A)
			HI	Arg217(A)
			PHI	Asp250(A), His251(A), Thr218(A), Ile256(A)
			π–sigma	Pro276(A)

DENV = Dengue virus; NS2B-NS3 = Nonstructural protein 2B–nonstructural protein 3 protease; vdw = van der Waals interactions; HI = Hydrophobic interactions; PHI = Hydrogen bond interactions; kcal/mol = Kilocalories per mole. Letters in parentheses identify protein chains. Quercetin served as the reference compound. Among the selected metabolites, 10-deoxymethynolide exhibited the most favorable predicted binding affinities.

The predicted molecular interactions between 10-deoxymethynolide and NS2B-NS3 proteins from the four DENV serotypes are presented in Figure 1.

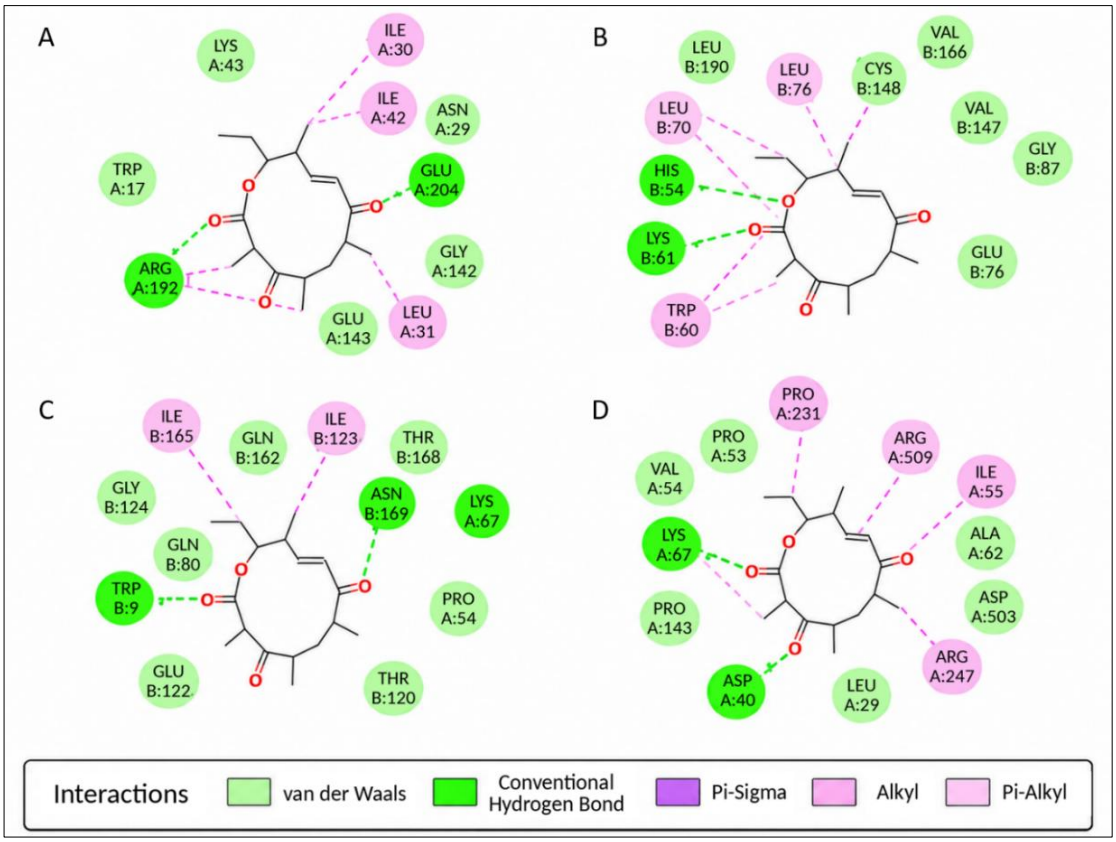


Figure 1: Predicted molecular interactions between 10-deoxymethynolide and the NS2B-NS3 proteases of four DENV serotypes. (A) 10-Deoxymethynolide–DENV-1 NS2B-NS3 complex; (B) 10-deoxymethynolide–DENV-2 NS2B-NS3 complex; (C) 10-deoxymethynolide–DENV-3 NS2B-NS3 complex; and (D) 10-deoxymethynolide–DENV-4 NS2B-NS3 complex. DENV = Dengue virus; NS2B-NS3 = Nonstructural protein 2B–nonstructural protein 3 protease.

The DENV-1 complex exhibited an RMSF value of 2.178 Å, followed by DENV-2 (2.281 Å), DENV-3 (1.963 Å), and DENV-4 (1.789 Å).

Among the four complexes, DENV-4 exhibited the lowest RMSF value, whereas DENV-2 exhibited the highest. These findings indicated differences in predicted residue-level fluctuations among the four NS2B-NS3 complexes. The corresponding RMSF profiles are presented in Figure 2.

doi: 10.14202/vetworld.2026.5088-5110

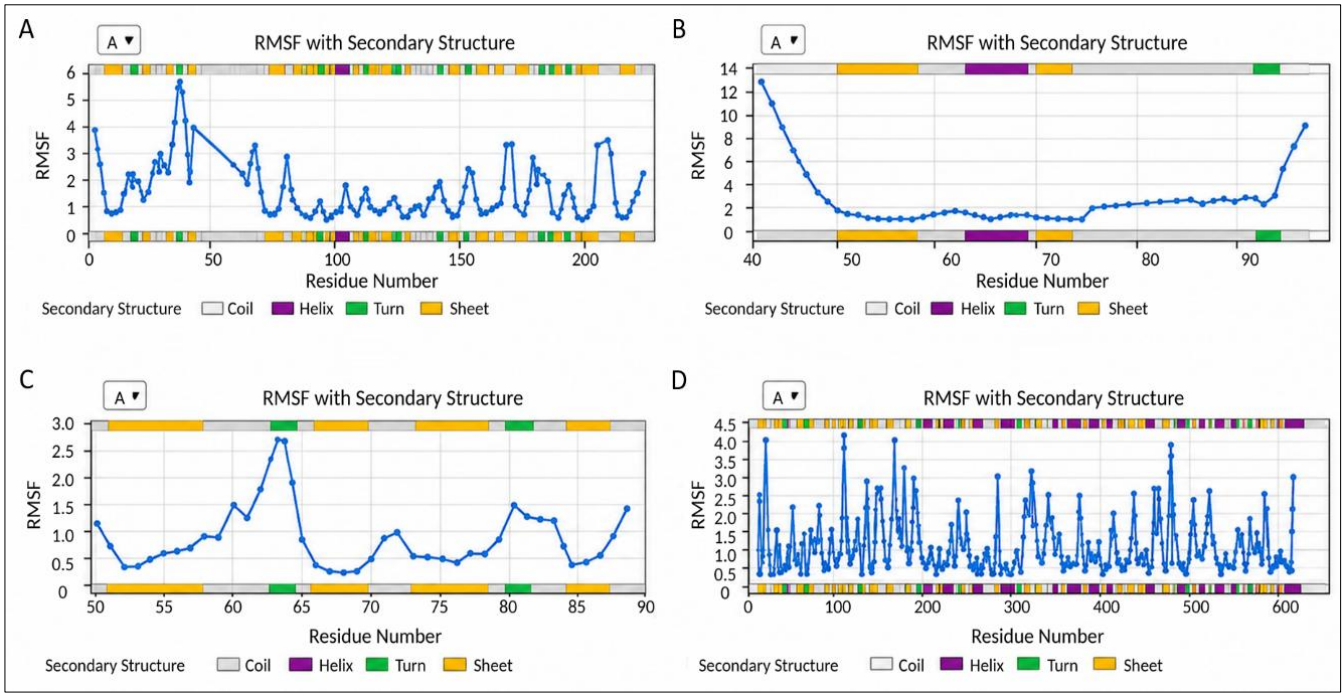


Figure 2: RMSF analysis of the 10-deoxymethynolide–NS2B-NS3 complexes across four DENV serotypes. (A) DENV-1 complex (RMSF = 2.178 Å); (B) DENV-2 complex (RMSF = 2.281 Å); (C) DENV-3 complex (RMSF = 1.963 Å); and (D) DENV-4 complex (RMSF = 1.789 Å). RMSF = Root mean square fluctuation; DENV = Dengue virus; NS2B-NS3 = Nonstructural protein 2B–nonstructural protein 3 protease; Å = Ångström.

Ramachandran plot analysis of NS2B-NS3 protein conformations

The stereochemical characteristics of NS2B-NS3 protein structures from the four DENV serotypes were assessed using Ramachandran plot analysis (Figure 3). The proportions of amino acid residues located within the favored, allowed, and disallowed regions were determined for each protein structure.

For DENV-2, 99.47% of residues were located in the favored region and 0.53% in the allowed region, with no residues in the disallowed region. Similarly, DENV-1 exhibited 96.81% of residues in the favored region and 3.20% in the allowed region, with no residues in the disallowed region.

For DENV-3, 96.25% of residues were located in the favored region, 3.51% in the allowed region, and 0.25% in the disallowed region. The corresponding proportions for DENV-4 were 90.35%, 8.67%, and 0.10%, respectively.

The Ramachandran plot distributions for all four NS2B-NS3 protein structures are presented in Figure 3.

Predicted ADME properties and toxicity profile

The predicted pharmacokinetic properties of 10-deoxymethynolide are presented in Table 6. The compound exhibited a predicted intestinal absorption of 95.563%, Caco-2 permeability of 1.102 log Papp (10^{-6} cm/s), water solubility of −3.058 log mol/L, and skin permeability of −3.642 log Kp.

Regarding distribution, the predicted unbound fraction was 0.432, whereas blood–brain barrier permeability and central nervous system permeability were 0.090 log BB and −2.802 log PS, respectively.

Metabolic predictions in cytochrome family protein (CYP) indicated that 10-deoxymethynolide was neither a substrate nor an inhibitor of CYP2D6 or CYP3A4. The compound was also predicted not to inhibit CYP1A2, CYP2C19, CYP2C9, CYP2D6, or CYP3A4. Its predicted total clearance was 1.414 log mL/min/kg, and it was not identified as a substrate of the renal organic cation transporter (OCT2) transporter.

Toxicity prediction classified 10-deoxymethynolide as toxicity class V, with a predicted median lethal dose (LD50) of 5000 mg/kg. The compound was predicted to be negative for nutritoxicity, cardiotoxicity, mutagenicity, ecotoxicity, neurotoxicity, hepatotoxicity, cytotoxicity, carcinogenicity, and respiratory toxicity. Positive predictions were obtained for nephrotoxicity, blood–brain barrier penetration, and immunotoxicity (Figure 4).

Cytotoxicity assessment of *Z. officinale* extract

The cytotoxicity assay demonstrated a concentration-dependent reduction in Vero cell viability following exposure to *Z. officinale* ethanolic extract. Increasing extract concentrations were associated with progressively lower OD values and cell viability percentages (Table 7 and Figure 5).

doi: 10.14202/vetworld.2026.5088-5110

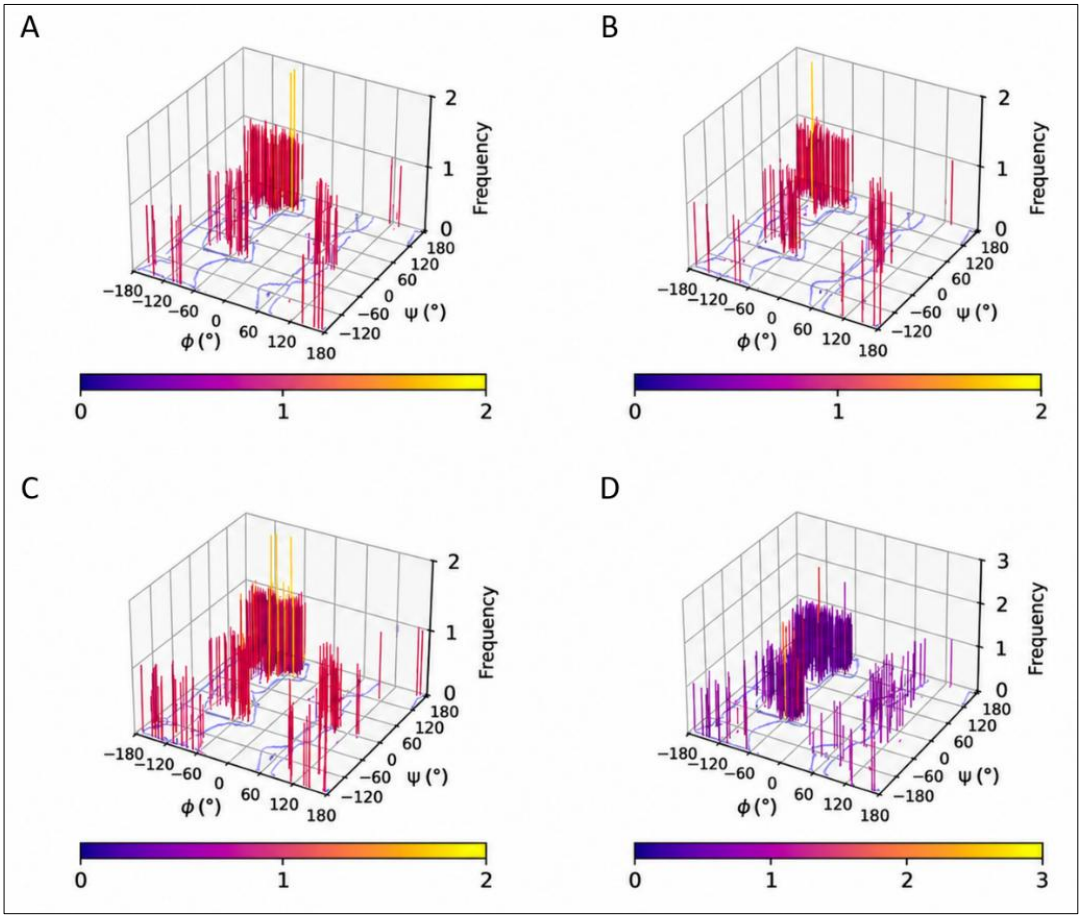


Figure 3: Ramachandran plot analysis of NS2B-NS3 protein structures from four DENV serotypes. (A) DENV-1: Favored region = 96.81%, allowed region = 3.20%, and disallowed region = 0%; (B) DENV-2: Favored region = 99.47%, allowed region = 0.53%, and disallowed region = 0%; (C) DENV-3: Favored region = 96.25%, allowed region = 3.51%, and disallowed region = 0.25%; and (D) DENV-4: Favored region = 90.35%, allowed region = 8.67%, and disallowed region = 0.10%. DENV = Dengue virus; NS2B-NS3 = Nonstructural protein 2B–nonstructural protein 3 protease.

Table 6: Predicted ADME properties of 10-deoxymethynolide.

Category	Parameter	Predicted value	Unit
Absorption	Water solubility	−3.058	log mol/L
	Caco-2 permeability	1.102	log Papp (10^{-6} cm/s)
	Intestinal absorption (human)	95.563	% absorbed
	Skin permeability	−3.642	log Kp
	P-glycoprotein substrate	No	Category (Yes/No)
	P-glycoprotein I inhibition	No	Category (Yes/No)
	P-glycoprotein II inhibition	No	Category (Yes/No)
Distribution	VDss (human)	−0.094	log L/kg
	Fraction unbound (human)	0.432	Fu
	BBB permeability	0.090	log BB
	CNS permeability	−2.802	log PS
Metabolism	CYP2D6 substrate	No	Category (Yes/No)
	CYP3A4 substrate	No	Category (Yes/No)
	CYP1A2 inhibition	No	Category (Yes/No)
	CYP2C19 inhibition	No	Category (Yes/No)
	CYP2C9 inhibition	No	Category (Yes/No)
	CYP2D6 inhibition	No	Category (Yes/No)
	CYP3A4 inhibition	No	Category (Yes/No)
Excretion	Total clearance	1.414	log mL/min/kg
	Renal OCT2 substrate	No	Category (Yes/No)

ADME = Absorption, distribution, metabolism, and excretion; Caco-2 = Human colorectal adenocarcinoma cell line; Papp = Apparent permeability coefficient; Kp = Skin permeability coefficient; VDss = Volume of distribution at steady state; Fu = Fraction unbound; BBB = Blood–brain barrier; CNS = Central nervous system; CYP = Cytochrome P450; OCT2 = Organic cation transporter 2. All values represent computational predictions.

doi: 10.14202/vetworld.2026.5088-5110

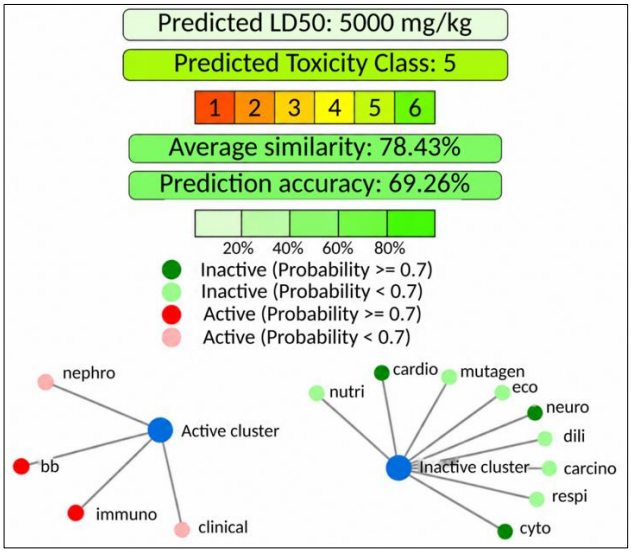


Figure 4: Predicted toxicity profile of 10-deoxymethynolide obtained using the ProTox 3.0 web server. The analysis presents computational toxicity predictions for the evaluated endpoints, including organ toxicity and other toxicological properties. The results represent computational predictions rather than experimentally confirmed toxicity.

Table 7: Cytotoxicity of *Zingiber officinale* ethanolic extract and quercetin in Vero cells.

Concentration (µg/mL)	*Z. officinale* extract: Mean OD ± SD	*Z. officinale* extract: Cell viability (%)	Quercetin: Mean OD ± SD	Quercetin: Cell viability (%)
31.25	0.099 ± 0.0017	86.458	0.167 ± 0.0010	91.549
62.5	0.095 ± 0	73.958	0.155 ± 0.0010	81.126
125	0.093 ± 0	67.708	0.147 ± 0.0030	74.085
250	0.091 ± 0.0005	63.541	0.141 ± 0.0030	69.296
500	0.076 ± 0.0011	16.667	0.136 ± 0.0030	65.296
1000	0.073 ± 0.0011	7.291	0.129 ± 0.0070	59.154
Cell control	0.103 ± 0.0005	—	0.071 ± 0.0015	—
Medium-control	0.071 ± 0.0015	—	0.059 ± 0.0000	—
CC_{50} (µg/mL)	—	359.93	—	1212.30

OD = Optical density; SD = Standard deviation; CC_{50} = 50% cytotoxic concentration. Values are expressed as mean ± SD from three technical replicates (n = 3). CC_{50} was reported as calculated by 44L nonlinear regression of percentage cell viability against concentration. — = Not applicable.

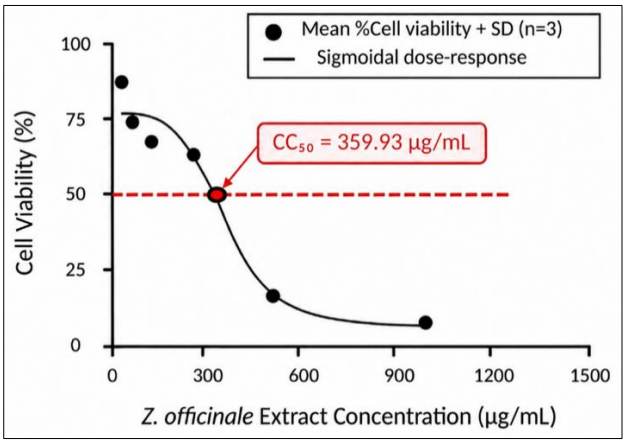


Figure 5: Concentration-dependent cytotoxic effects of *Zingiber officinale* extract on Vero E6 cells. Cell viability was assessed at extract concentrations of 31.25, 62.5, 125, 250, 500, and 1000 µg/mL. Bars represent mean percentage cell viability ± SD from three technical replicates (n = 3) within a single independent experiment. The concentration–response curve was fitted using a four-parameter logistic (4PL) nonlinear regression model. The estimated 50% cytotoxic concentration (CC_{50}) was 359.93 µg/mL (Table 7). SD = Standard deviation; 4PL = Four-parameter logistic; CC_{50} = 50% cytotoxic concentration.

At concentrations of 31.25–250 µg/mL, cell viability ranged from 63.541% to 86.458%, indicating that a substantial proportion of cells retained metabolic activity following treatment.

At higher concentrations, cell viability decreased markedly. Treatment with 500 µg/mL extract reduced cell viability to 16.667%, whereas exposure to 1000 µg/mL resulted in 7.291% viability. These findings indicated

pronounced cytotoxic effects at the highest tested concentrations.

The estimated CC_{50} of the extract was 359.93 µg/mL. Cell viability decreased substantially at concentrations exceeding this value, demonstrating the concentration-dependent cytotoxicity of the extract under the experimental conditions.

Anti-dengue activity across the four DENV serotypes

The anti-dengue assay showed concentration-dependent changes in CPE percentages across the four DENV serotypes (Table 8).

Table 8: Anti-dengue assay results for *Zingiber officinale* ethanolic extract and quercetin across four DENV serotypes, measured by cytopathic effect.

Serotype/concentration	*Z. officinale* extract: Mean OD	*Z. officinale* extract: CPE (%)	Quercetin: Mean OD	Quercetin: CPE (%)
DENV-1				
6.25 µg/mL	2.21×10^7	110.25	3.61×10^7	82.81
12.5 µg/mL	2.14×10^7	106.88	3.43×10^7	78.60
25 µg/mL	2.07×10^7	103.55	3.06×10^7	70.24
50 µg/mL	2.02×10^7	100.62	2.95×10^7	67.57
100 µg/mL	1.95×10^7	97.49	2.18×10^7	49.92
DENV-1 + Cell control	2.00×10^7	—	4.36×10^7	—
Medium-control	2.90×10^3	—	4.32×10^3	—
EC_{50} (µg/mL)	—	479.03	—	99.31
SI (CC_{50}/EC_{50})	—	0.75	—	12.21
DENV-2				
6.25 µg/mL	3.90×10^7	98.84	3.46×10^7	85.94
12.5 µg/mL	3.73×10^7	94.45	3.31×10^7	82.26
25 µg/mL	3.62×10^7	91.58	3.12×10^7	77.44
50 µg/mL	3.55×10^7	89.89	2.91×10^7	72.33
100 µg/mL	3.45×10^7	87.26	2.25×10^7	55.86
DENV-2 + Cell control	3.95×10^7	—	4.03×10^7	—
Medium-control	4.99×10^3	—	4.32×10^3	—
EC_{50} (µg/mL)	—	452.87	—	119.53
SI (CC_{50}/EC_{50})	—	0.79	—	10.14
DENV-3				
6.25 µg/mL	2.94×10^7	109.05	3.32×10^7	83.16
12.5 µg/mL	2.86×10^7	106.10	3.21×10^7	80.36
25 µg/mL	2.77×10^7	102.77	3.06×10^7	76.60
50 µg/mL	2.74×10^7	101.38	2.86×10^7	71.63
100 µg/mL	2.56×10^7	94.81	2.33×10^7	58.36
DENV-3 + Cell control	2.70×10^7	—	4.00×10^7	—
Medium-control	3.90×10^3	—	4.32×10^3	—
EC_{50} (µg/mL)	—	425.16	—	132.81
SI (CC_{50}/EC_{50})	—	0.84	—	9.12
DENV-4				
6.25 µg/mL	2.50×10^7	99.81	3.04×10^7	88.93
12.5 µg/mL	2.44×10^7	97.46	2.88×10^7	84.22
25 µg/mL	2.35×10^7	93.75	2.76×10^7	80.71
50 µg/mL	2.27×10^7	90.66	2.62×10^7	76.58
100 µg/mL	2.21×10^7	88.17	1.90×10^7	55.59
DENV-4 + Cell control	2.50×10^7	—	3.42×10^7	—
Medium-control	3.31×10^3	—	4.32×10^3	—
EC_{50} (µg/mL)	—	419.78	—	120.05
SI (CC_{50}/EC_{50})	—	0.85	—	10.09

DENV = Dengue virus; OD = Optical density; CPE = Cytopathic effect; EC_{50} = 50% effective concentration; CC_{50} = 50% cytotoxic concentration; SI = Selectivity index (CC_{50}/EC_{50}); SD = Standard deviation. Measurements were performed in three technical replicates (n = 3). EC_{50} was reported as calculated by linear regression of percentage CPE against concentration. — = Not applicable.

For DENV-1, CPE decreased from 110.25% at 6.25 µg/mL to 97.49% at 100 µg/mL. The estimated EC_{50} was 479.03 µg/mL, with an SI of 0.75.

For DENV-2, CPE decreased from 98.84% at 6.25 µg/mL to 87.26% at 100 µg/mL. The estimated EC_{50} and SI were 452.87 µg/mL and 0.79, respectively.

For DENV-3, CPE decreased from 109.05% to 94.81% across the tested concentration range. The estimated EC_{50} was 425.16 µg/mL, with an SI of 0.84.

For DENV-4, CPE decreased from 99.81% at the lowest concentration to 88.17% at the highest concentration. The estimated EC_{50} was 419.78 µg/mL, with an SI of 0.85. Among the four serotypes, DENV-4 generally exhibited lower CPE percentages across the tested concentrations.

All estimated EC_{50} values exceeded the maximum experimentally tested extract concentration of 100 µg/mL. Therefore, these estimates were extrapolated beyond the observed concentration–response range, and 50% antiviral effectiveness was not demonstrated within the tested concentrations.

Quercetin was included as a reference antiviral control to contextualize the *in vitro* anti-DENV activity. Quercetin exhibited EC_{50} values ranging from 99.31 to 132.81 µg/mL and SI values ranging from 9.12 to 12.21 across the four serotypes. In comparison, the *Z. officinale* crude extract exhibited substantially lower SI values, indicating less favorable selectivity between antiviral-associated effects and cytotoxicity under the experimental conditions.

DISCUSSION

Phytochemical diversity of *Z. officinale* extract

The present study evaluated the potential anti-dengue activity of *Z. officinale* ethanolic extract against four DENV serotypes by integrating LC-HRMS-based metabolite profiling, computational screening, molecular docking, protein flexibility analysis, ADME and toxicity predictions, and *in vitro* cytotoxicity and antiviral-associated assays. This integrated approach provided complementary information on the phytochemical composition, predicted molecular interactions, and biological effects of the crude extract [23]. However, the computational predictions and cell-based findings represent different levels of evidence and should be interpreted accordingly.

LC-HRMS analysis yielded 45 putatively annotated metabolites belonging to several chemical classes, including terpenoids, phenolic compounds, steroids, alkaloids, and fatty acid derivatives. The presence of several terpenoid-associated metabolites is consistent with previous reports describing ginger rhizomes as sources of sesquiterpenes and monoterpenes with potential antiviral, anti-inflammatory, and immunomodulatory activities [4]. Samy *et al.* [24] reported that ginger-derived compounds, including gingerdiacetate, may exhibit antiviral activity through interactions with viral proteins and modulation of host cellular responses. These findings provide a rationale for investigating ginger metabolites as potential antiviral agents. Nevertheless, the present LC-HRMS results represent putative metabolite annotations and do not establish the antiviral activity of individual constituents.

Drug-likeness and predicted antiviral potential of putatively annotated metabolites

Among the putatively annotated metabolites, α-farnesene exhibited the highest predicted antiviral probability in the PASS analysis. This compound belongs to the sesquiterpene hydrocarbon group, which has been associated with antioxidant and antiviral activities against several RNA viruses. However, molecular docking indicated that α-farnesene exhibited less favorable predicted binding affinities toward NS2B-NS3 proteases than 10-deoxymethynolide.

This difference suggests that a high predicted probability of antiviral activity does not necessarily correspond to favorable binding affinity toward a specific viral protein. Rasool *et al.* [25] similarly reported that some phytochemicals with high predicted biological activity exhibited moderate docking performance, potentially because of limited polar interactions with protein residues. The predominantly hydrophobic structure of α-farnesene may restrict its ability to form hydrogen bonds within the protease binding region.

The selection of metabolites in the present study was primarily guided by PASS-predicted antiviral potential. Consequently, the selected compounds should be regarded as candidates prioritized through computational screening rather than as a definitive ranking of the biological importance of all metabolites present in the extract.

Molecular docking analysis against NS2B-NS3 proteases

Among the three selected metabolites, 10-deoxymethynolide exhibited the most favorable predicted binding affinities across the four DENV serotypes. Its docking scores ranged from −6.5 to −7.2 kcal/mol, with the most favorable value observed against DENV-4 (−7.2 kcal/mol). Although these values were less favorable than those of the positive control, quercetin, they suggest that 10-deoxymethynolide warrants further investigation as a potential NS2B-NS3-interacting compound [26].

The predicted interactions may be influenced by the structural flexibility of 10-deoxymethynolide and the

presence of oxygen-containing functional groups, which could facilitate hydrophobic, van der Waals, and hydrogen bond interactions within the protein binding region.

The NS2B-NS3 protease is an important target for dengue antiviral development because of its role in viral polyprotein processing and the maturation of proteins required for viral replication [10]. Tahir *et al.* [27] reported that NS2B-NS3 inhibitors commonly interact with catalytic residues, including His51, Asp75, and Ser135. In the present study, 10-deoxymethynolide exhibited predicted interactions with residues in the NS2B-NS3 binding regions of all four DENV serotypes. However, molecular docking alone cannot establish direct protease inhibition, and the predicted interactions require experimental confirmation.

The comparative analysis across four DENV serotypes represents an important feature of this study. Previous computational investigations have frequently focused on individual serotypes, particularly DENV-2. Because structural differences among serotypes may influence ligand-binding, evaluating all four serotypes provides a broader preliminary assessment of potential cross-serotype interactions.

The relatively consistent docking scores of 10-deoxymethynolide suggest its potential for further investigation as a cross-serotype NS2B-NS3 inhibitor. Lee *et al.* [28] emphasized the importance of developing antiviral strategies that provide activity across DENV serotypes, particularly given the clinical challenges associated with secondary dengue infections and ADE. Nevertheless, the present docking results do not demonstrate pan-serotype antiviral efficacy.

Conformational dynamics of ligand–NS2B-NS3 complexes

The protein flexibility analysis provided additional information on the predicted conformational behavior of the selected NS2B-NS3 structures. Among the four evaluated serotypes, the DENV-4 complex showed the lowest RMSF, indicating lower predicted residue-level fluctuations, whereas the DENV-2 complex showed the highest RMSF.

Lower RMSF values generally indicate reduced local structural fluctuations within the analyzed model. Previous studies have discussed the potential relevance of protein flexibility and conformational stability in evaluating protein–ligand interactions [29, 30]. However, RMSF values alone do not establish the persistence of ligand-binding or the biological stability of a protein–ligand complex.

Therefore, the present results should be interpreted as preliminary computational evidence of differences in predicted protein flexibility rather than definitive validation of stable ligand–protease interactions under physiological conditions.

Ramachandran plot analysis of NS2B-NS3 protein conformations

Ramachandran plot analysis showed that most amino acid residues in the NS2B-NS3 protein structures were located within the favored conformational regions. This finding indicates generally acceptable backbone stereochemical characteristics of the evaluated protein structures.

Stereochemical assessment is important in computational studies because structural inaccuracies may influence the interpretation of predicted molecular interactions [28, 31]. Heo and Feig [32] emphasized the relevance of protein structural quality in computational modeling, while other studies have highlighted the importance of structural validation before molecular docking and simulation analyses [33, 34].

Although the predominance of residues in favored regions supports the stereochemical suitability of the evaluated structures, Ramachandran plot analysis alone cannot confirm the accuracy of ligand-binding predictions or the biological relevance of the docking results.

Predicted ADME properties and toxicity profile

The computational assessment indicated that 10-deoxymethynolide satisfied the evaluated Lipinski Ro5 criteria and exhibited favorable predicted intestinal absorption and membrane permeability. These characteristics suggest potentially suitable drug-likeness properties for further investigation.

Pharmacokinetic characteristics are important considerations during drug development because compounds with promising biological activity may fail to progress because of inadequate absorption, distribution, metabolism, or elimination profiles. Daina *et al.* [35] emphasized the importance of early pharmacokinetic screening in identifying potential drug candidates. Similarly, previous studies have highlighted the relevance of membrane permeability and cytochrome P450 interactions in evaluating candidate compounds [36].

However, satisfying Lipinski Ro5 criteria and obtaining favorable computational ADME predictions do not establish actual oral bioavailability, clinical safety, or therapeutic effectiveness. Experimental pharmacokinetic

studies are required to determine the absorption, distribution, metabolism, and elimination characteristics of 10-deoxymethynolide.

The toxicity assessment classified 10-deoxymethynolide as toxicity class V, with a predicted LD50 of 5000 mg/kg. The compound was also predicted to be negative for mutagenicity and carcinogenicity, suggesting a potentially favorable preliminary toxicity profile for these endpoints. However, positive predictions for nephrotoxicity and immunotoxicity indicate potential safety concerns that require further evaluation.

Valerio [37] highlighted the role of computational toxicology in identifying potential hazards during early drug discovery. Kar and Leszczynski [38] similarly emphasized that computational toxicity predictions require experimental validation before conclusions regarding physiological safety can be established.

Accordingly, the ADME and toxicity results should be considered preliminary screening findings rather than evidence of the compound's safety or suitability for therapeutic use.

Cytotoxicity assessment of *Z. officinale* extract

The cytotoxicity assay demonstrated a concentration-dependent reduction in Vero cell viability following treatment with *Z. officinale* ethanolic extract. At concentrations of 31.25–250 µg/mL, cell viability remained between 63.541% and 86.458%, indicating that a substantial proportion of cells retained metabolic activity after exposure.

In contrast, treatment with 500 and 1000 µg/mL reduced cell viability to 16.667% and 7.291%, respectively. The estimated CC_{50} of 359.93 µg/mL further indicated that cytotoxicity increased with extract concentration.

These findings suggest that the biological effects of the crude extract depend strongly on the administered concentration. Chang *et al.* [39] previously reported antiviral activity of fresh ginger extract against human respiratory syncytial virus in HEp-2 and A549 cells, together with concentration-dependent effects on cell viability. Although that study involved a different viral system, it provides supporting context for the importance of evaluating both antiviral-associated effects and host-cell cytotoxicity.

The diverse phytochemical composition of the extract may contribute to its concentration-dependent cytotoxicity. Terpenoid and phenolic compounds have been associated with biological effects involving cellular membranes and oxidative stress pathways [4]. However, the present study did not directly investigate membrane integrity, oxidative stress, or mechanisms of cell death. Therefore, the observed cytotoxicity cannot be attributed to specific metabolites or cellular mechanisms based on the available results.

Anti-dengue activity across the four DENV serotypes

The antiviral-associated assay showed concentration-dependent reductions in CPE percentages across all four DENV serotypes following treatment with *Z. officinale* ethanolic extract. These observations suggest that extract exposure influenced the cellular response to DENV infection under the experimental conditions.

However, the results require cautious interpretation because the assay measured cellular viability and virus-associated CPE rather than directly quantifying viral replication. Consequently, the observed reductions in CPE cannot independently establish inhibition of DENV replication.

The estimated SI values were 0.75, 0.79, 0.84, and 0.85 for DENV-1, DENV-2, DENV-3, and DENV-4, respectively. These values were substantially lower than those obtained for the quercetin control (9.12–12.21), indicating limited separation between antiviral-associated effects and host-cell cytotoxicity.

Furthermore, the estimated EC_{50} values for the extract exceeded the maximum experimentally tested concentration of 100 µg/mL. Therefore, the EC_{50} estimates were extrapolated beyond the observed concentration–response range, and 50% antiviral effectiveness was not demonstrated within the tested concentrations.

Although an SI above 10 is sometimes used as a preliminary indicator of favorable antiviral selectivity, such thresholds depend on the assay system and the compound being evaluated. The SI values obtained in the present study indicate that the crude extract did not demonstrate favorable antiviral selectivity under the experimental conditions.

The low selectivity may partly reflect the complex phytochemical composition of the crude extract, which contains multiple metabolites with potentially different biological activities. However, the presence of numerous constituents does not independently explain or justify the observed low SI values.

Bioassay-guided fractionation and purification may help determine whether specific antiviral constituents can be separated from components responsible for cytotoxicity. Previous studies have reported that fractionation or isolation of bioactive constituents may improve antiviral potency and selectivity compared with crude preparations [40–42].

Accordingly, the present findings should be interpreted as preliminary evidence of concentration-dependent changes in DENV-associated CPE rather than evidence of selective antiviral efficacy or therapeutic potential of the crude extract.

The computational findings provide a complementary basis for further investigation. Among the putatively annotated metabolites, 10-deoxymethynolide exhibited relatively favorable predicted binding affinities toward NS2B-NS3 proteins from all four DENV serotypes.

Nevertheless, these predictions should be considered separately from the limited selectivity observed in the crude extract assay. Favorable predicted binding of 10-deoxymethynolide does not establish that this compound was responsible for the observed cellular effects or that it inhibits NS2B-NS3 protease activity.

Experimental evaluation of purified compounds or enriched fractions, together with direct viral replication and protease inhibition assays, is therefore necessary to determine whether the selected metabolites possess selective anti-DENV activity.

Strengths, limitations, and future directions

An important strength of the present study was the integration of LC-HRMS-based metabolite profiling, computational screening, molecular docking, protein flexibility analysis, and *in vitro* assays across all four DENV serotypes. This approach enabled the preliminary identification of putatively annotated metabolites with predicted antiviral potential while simultaneously evaluating the biological limitations of the crude extract.

The inclusion of all four DENV serotypes provided a broader comparative assessment than investigations restricted to a single serotype. In addition, the combined evaluation of cytotoxicity and antiviral-associated effects allowed the selectivity of the crude extract to be assessed rather than relying solely on changes in virus-associated cellular responses.

Nevertheless, several limitations should be considered. First, the use of a crude ethanolic extract prevented the biological effects from being attributed to individual metabolites. Although α-farnesene, muramic acid, and 10-deoxymethynolide exhibited favorable computational screening results, their presence was based on putative LC-HRMS annotations, and their individual antiviral activities were not experimentally confirmed.

Future investigations should therefore include metabolite confirmation, bioassay-guided fractionation, purification, and testing of isolated compounds to identify constituents with improved antiviral selectivity.

Second, the study used Vero cells, which are widely employed in virological research because of their permissiveness to viral infection. However, these cells lack a complete type I interferon response, which may influence their response to viral infection and antiviral compounds.

Further evaluation using human-derived cell models, including Huh7, HepG2, or monocyte-derived cells, may provide additional information on the biological relevance of the observed effects.

Third, the multiplicity of infection was not experimentally determined or used as a predefined assay parameter. Instead, the antiviral experiments were standardized using infectious viral titers. Although the viral input was quantified using an FFU-based assay, viral replication following treatment was not directly measured.

The antiviral endpoint was based on CPE and cell viability. Therefore, the observed effects should not be interpreted as definitive evidence of direct inhibition of viral replication. Future studies should incorporate direct viral quantification methods to determine whether treatment reduces viral replication or infectious virus production. The important limitation of the MTT assay is that it measures cellular metabolic activity as an indirect indicator of cell viability rather than directly assessing plasma membrane integrity or the mechanism of cell death. Additional assays, such as membrane integrity assays or apoptosis-specific analyses, would be required to characterize this mechanism.

Fourth, the *in vitro* experiments were conducted using three technical replicates within a single independent experimental run rather than multiple independent biological experiments. Consequently, the findings primarily reflect within-experiment variability and do not adequately characterize between-experiment variation. Independent biological replication is required to establish the reproducibility of the observed effects. The concentration-response modeling was based on a single independent experiment with three technical replicates. Consequently, the estimated CC_{50} and EC_{50} values and their corresponding confidence intervals reflect the fitted model and the available technical data rather than biological variability across independent experiments. Therefore, these estimates should be interpreted as exploratory and require confirmation through additional independent biological experiments.

Fifth, the molecular docking results represent computational estimates of ligand–protein binding affinity and

do not directly demonstrate NS2B-NS3 protease inhibition. An important limitation of the molecular docking analysis is the absence of conventional docking validation through redocking of co-crystallized organic ligands for this purpose; the associated components were inorganic ions. Therefore, RMSD-based validation of the docking protocol could not be performed. Accordingly, the predicted binding interactions should be considered hypothesis-generating and require further validation through appropriate benchmark compounds and experimental protease inhibition assays. Similarly, the protein flexibility analysis performed using CABS-flex 3.0 provides a coarse-grained assessment of predicted conformational fluctuations rather than comprehensive evidence of ligand–protein complex stability. Therefore, the RMSF findings should be interpreted cautiously and considered supportive computational observations rather than definitive evidence of complex stability.

Further computational investigations using all-atom molecular dynamics simulations, clearly defined simulation parameters, independent replicates, and complementary trajectory-based analyses may provide a more detailed assessment of the predicted binding behavior and conformational dynamics of the selected complexes.

The principal contribution of this study lies in its integrated evaluation of *Z. officinale* ethanolic extract across four DENV serotypes. Previous investigations of the antiviral properties of *Z. officinale* have primarily focused on respiratory viruses, including human respiratory syncytial virus, influenza virus, and severe acute respiratory syndrome coronavirus 2, whereas studies addressing its potential anti-dengue activity across multiple serotypes remain limited.

The present findings identify 10-deoxymethynolide as a computationally prioritized metabolite for further investigation while demonstrating that the crude extract has limited antiviral selectivity under the tested conditions.

Therefore, the study provides a preliminary framework for identifying and evaluating potentially active constituents of *Z. officinale*, rather than establishing the extract as an effective or selective anti-dengue agent. Future research should prioritize the experimental confirmation of putative metabolites, identification of selective antiviral constituents, direct assessment of viral replication and protease inhibition, and independent validation of biological activity.

CONCLUSION

The present study integrated LC-HRMS-based metabolite profiling, *in silico* analyses, and *in vitro* assays to evaluate the potential anti-dengue activity of *Z. officinale* ethanolic extract against four DENV serotypes. LC-HRMS analysis identified 45 putatively annotated metabolites, and computational screening prioritized α-farnesene, muramic acid, and 10-deoxymethynolide. Of these, 10-deoxymethynolide exhibited the most favorable predicted binding affinities toward NS2B-NS3 proteases across the four DENV serotypes, particularly DENV-4 (−7.2 kcal/mol). However, the crude extract exhibited concentration-dependent cytotoxicity (CC_{50} = 359.93 µg/mL) and low antiviral selectivity (SI = 0.75–0.85). Furthermore, all estimated EC_{50} values exceeded the maximum tested concentration of 100 µg/mL, indicating that 50% antiviral effectiveness was not demonstrated within the evaluated concentration range.

The findings suggest that *Z. officinale* may provide a source of metabolites for further antiviral screening. In particular, 10-deoxymethynolide represents a computationally prioritized candidate for experimental investigation. However, the low SI values indicate that the crude ethanolic extract is not currently a selective anti-dengue agent. Future development should focus on identifying individual constituents with improved antiviral activity and reduced host-cell cytotoxicity.

Although *Z. officinale* ethanolic extract produced concentration-dependent changes in DENV-associated CPE, its low antiviral selectivity limits its potential for direct therapeutic development. The computational findings identify 10-deoxymethynolide as a candidate for further investigation but do not establish its antiviral efficacy. Overall, this study provides a preliminary foundation for identifying and experimentally validating selective anti-dengue constituents from *Z. officinale*, rather than evidence supporting the crude extract as an effective antiviral treatment.

DATA AVAILABILITY

All data supporting the findings of this study are included in the manuscript, including the processed LC-HRMS data, metabolite annotations, relevant assay datasets, and docking coordinates. The docking structures and

input files used for the computational analyses are available from the corresponding author upon reasonable request.

GENERATIVE AI DECLARATION

The authors declare that no generative artificial intelligence (AI) tools were used in the preparation, writing, data analysis, or interpretation of this manuscript. All scientific content and conclusions were developed and reviewed b the authors, who take full resppnsibility for the accuracy and integrity of the work.

AUTHORS' CONTRIBUTIONS

MAH, WDM, DWN, and RAD: Conceptualization, study design, and materials. WDM, DWN, and RAD: Supervision and resources. MAH, PAI, and THS: Data collection and literature search. MAH, PAI, AUR, RAR, RJK, and PAW: Data analysis and interpretation. MAH, PAI, and AUR: Data visualization. MAH, WDM, DWN, PAI, and AUR: Manuscript drafting. RAD: Critical review and revision of the manuscript. All authors read and approved the final manuscript.

ACKNOWLEDGMENTS

This study was supported by the Program Magister Menuju Doktor untuk Sarjana Unggul (PMDSU) Scholarship Scheme, funded by the Ministry of Higher Education, Research, and Technology, Republic of Indonesia, under Contract No. 067/C3/DT.05.00/PL-MULTITAHUNLANJUTAN/2026 and Specific Contract No. 1115/B/DST/UN3.DRI/PT.01.03/2026.

COMPETING INTERESTS

The authors declare that they have no competing interests.

PUBLISHER'S NOTE

Veterinary World remains neutral with regard to jurisdictional claims in the published institutional affiliations.

REFERENCES

1. Lee MF, Wu YS, Poh CL. Molecular mechanisms of antiviral agents against dengue virus. Viruses. 2023;15:705.
2. Low ZX, OuYong BM, Hassandarvish P, Poh CL, Ramanathan B. Antiviral activity of silymarin and baicalein against dengue virus. Sci Rep. 2021;11:21221.
3. Panda K, Alagarasu K, Patil P, Agrawal M, More A, Kumar NV, *et al*. *In vitro* antiviral activity of α-mangostin against dengue virus serotype-2 (DENV-2). Molecules. 2021;26:3016.
4. Mao QQ, Xu XY, Cao SY, Gan RY, Corke H, Beta T, *et al*. Bioactive compounds and bioactivities of ginger (*Zingiber officinale* Roscoe). Foods. 2019;8:185.
5. Deng M, Yun X, Ren S, Qing Z, Luo F. Plants of the genus *Zingiber*: a review of their ethnomedicine, phytochemistry and pharmacology. Molecules. 2022;27:2826.
6. Alolga RN, Wang F, Zhang X, Li J, Tran L-SP, Yin X. Bioactive compounds from the Zingiberaceae family with known antioxidant activities for possible therapeutic uses. Antioxidants. 2022;11:1281.
7. Wijaya RM, Hafidzhah MA, Kharisma VD, Ansori ANM, Parikesit AA. COVID-19 *in silico* drug with *Zingiber officinale* natural product compound library targeting the Mpro protein. Makara J Sci. 2021;25.
8. Aceña J, Stampachiacchiere S, Pérez S, Barceló D. Advances in liquid chromatography-high-resolution mass spectrometry for quantitative and qualitative environmental analysis. Anal Bioanal Chem. 2015;407:6289–6299.
9. Ali S, Ali U, Safi K, Naz F, Jan MI, Iqbal Z, *et al*. *In silico* homology modeling of dengue virus non-structural 4B (NS4B) protein and its molecular docking studies using triterpenoids. BMC Infect Dis. 2024;24:688.
10. Nitsche C, Holloway S, Schirmeister T, Klein CD. Biochemistry and medicinal chemistry of the dengue virus protease. Chem Rev. 2014;114:11348–11381.
11. Noble CG, Shi P-Y. Structural biology of dengue virus enzymes: towards rational design of therapeutics. Antiviral Res. 2012;96:115–126.
12. Lipinski CA. Lead- and drug-like compounds: the rule-of-five revolution. Drug Discov Today Technol. 2004; 1:337–341.

13. Rahayu S, Rohmatika AU, Islamatasya U, Herdiansyah MA, Susilo RJK, Hayaza S, *et al*. Potential of *Ganoderma applanatum* extract as anticancer and immunomodulator in diethylnitrosamine-induced colon cancer. Trop J Nat Prod Res. 2025;9.
14. Herdiansyah MA, Rizaldy R, Alifiansyah MR, Fetty AJ, Anggraini D, Agustina N, *et al*. Molecular interaction analysis of ferulic acid (4-hydroxy-3-methoxycinnamic acid) as main bioactive compound from palm oil waste against MCF-7 receptors: an *in silico* study. Narra J. 2024;4:e775.
15. Alifiansyah MRT, Herdiansyah MA, Pratiwi RC, Pramesti RP, Hafsyah NW, Rania AP, *et al*. QSAR of acyl alizarin red biocompound derivatives of *Rubia tinctorum* roots and its ADMET properties as anti-breast cancer candidates against MMP-9 protein receptor: *in silico* study. Food Syst. 2024;7:312–320.
16. Herdiansyah M, Darmanto W, Winarni D, Rohmatika A, Putri R, Susilo R, *et al*. Decoding antidengue serotype-3 (DENV-3) mechanism of natural glycosides from *Alpinia purpurata*: molecular docking and *in vitro* insights into viral entry, cytokine storm modulation, and endogenous antioxidant defense activation. Open Vet J. 2026;16:2987.
17. C S, S DK, Ragunathan V, Tiwari P, A S, P BD. Molecular docking, validation, dynamics simulations, and pharmacokinetic prediction of natural compounds against the SARS-CoV-2 main-protease. J Biomol Struct Dyn. 2022;40:585–611.
18. Kumar M, Rathore RS. RamPlot: a webserver to draw 2D, 3D and assorted Ramachandran (ϕ, ψ) maps. J Appl Crystallogr. 2025;58:630–636.
19. Fatima S, Gupta P, Sharma S, Sharma A, Agarwal SM. ADMET profiling of geographically diverse phytochemical using chemoinformatic tools. Future Med Chem. 2020;12:69–87.
20. Klimoszek D, Jeleń M, Dołowy M, Morak-Młodawska B. Study of the lipophilicity and ADMET parameters of new anticancer diquinothiazines with pharmacophore substituents. Pharmaceuticals. 2024;17:725.
21. Banerjee P, Kemmler E, Dunkel M, Preissner R. ProTox 3.0: a webserver for the prediction of toxicity of chemicals. Nucleic Acids Res. 2024;52:W513–520.
22. Wiradana PA, Wiartini NWAW, Sucipto TH, Herdiansyah MA, Permatasari AAAP, Widhiantara IG, *et al*. Evaluation of mangrove, *Acanthus ilicifolius* aqueous extract on inhibition of dengue virus replication: *in vitro* and molecular docking approach. Indones J Trop Infect Dis. 2025;13:251–266.
23. Asiamah I, Obiri SA, Tamekloe W, Armah FA, Borquaye LS. Applications of molecular docking in natural products-based drug discovery. Sci African. 2023;20:e01593.
24. Samy A, Hassan A, Hegazi NM, Farid M, Elshafei M. Network pharmacology, molecular docking, and dynamics analyses to predict the antiviral activity of ginger constituents against coronavirus infection. Sci Rep. 2024; 14:12059.
25. Qaddir I, Rasool N, Hussain W, Mahmood S. Computer-aided analysis of phytochemicals as potential dengue virus inhibitors based on molecular docking, ADMET and DFT studies. J Vector Borne Dis. 2017;54:255.
26. Ullah A, Atia-tul-Wahab, Gong P, Khan AM, Choudhary MI. Identification of new inhibitors of NS5 from dengue virus using saturation transfer difference (STD-NMR) and molecular docking studies. RSC Adv. 2023; 13:355–369.
27. Tahir ul QM, Kiran S, Ashfaq UA, Javed MR, Anwar F, Ali MA, *et al*. Discovery of novel dengue NS2B/NS3 protease inhibitors using pharmacophore modeling and molecular docking based virtual screening of the ZINC database. Int J Pharmacol. 2016;12:621–632.
28. Lee GR, Heo L, Seok C. Effective protein model structure refinement by loop modeling and overall relaxation. Proteins Struct Funct Bioinforma. 2016;84:293–301.
29. Patel CN, Jani SP, Jaiswal DG, Kumar SP, Mangukia N, Parmar RM, *et al*. Identification of antiviral phytochemicals as a potential SARS-CoV-2 main protease (Mpro) inhibitor using docking and molecular dynamics simulations. Sci Rep. 2021;11:20295.
30. Saqallah FG, Abbas MA, Wahab HA. Recent advances in natural products as potential inhibitors of dengue virus with a special emphasis on NS2b/NS3 protease. Phytochemistry. 2022;202:113362.
31. Heo L, Feig M. What makes it difficult to refine protein models further via molecular dynamics simulations? Proteins Struct Funct Bioinforma. 2018;86:177–188.
32. Heo L, Feig M. Experimental accuracy in protein structure refinement via molecular dynamics simulations. Proc Natl Acad Sci. 2018;115:13276–13281.
33. Abrams C, Bussi G. Enhanced sampling in molecular dynamics using metadynamics, replica-exchange, and

temperature-acceleration. Entropy. 2013;16:163–199.
34. Huang J, Rauscher S, Nawrocki G, Ran T, Feig M, de Groot BL, *et al*. CHARMM36m: an improved force field for folded and intrinsically disordered proteins. Nat Methods. 2017;14:71–73.
35. Daina A, Michielin O, Zoete V. SwissADME: a free web tool to evaluate pharmacokinetics, drug-likeness and medicinal chemistry friendliness of small molecules. Sci Rep. 2017;7:42717.
36. Pires DEV, Blundell TL, Ascher DB. pkCSM: predicting small-molecule pharmacokinetic and toxicity properties using graph-based signatures. J Med Chem. 2015;58:4066–4072.
37. Valerio Jr LG. *In silico* toxicology for the pharmaceutical sciences. Toxicol Appl Pharmacol. 2009;241:356–370.
38. Kar S, Leszczynski J. Exploration of computational approaches to predict the toxicity of chemical mixtures. Toxics. 2019;7:15.
39. Chang JS, Wang KC, Yeh CF, Shieh DE, Chiang LC. Fresh ginger (*Zingiber officinale*) has anti-viral activity against human respiratory syncytial virus in human respiratory tract cell lines. J Ethnopharmacol. 2013;145:146–151.
40. Herdiansyah MA, Darmanto W, Winarni D, Doong R, Tory Alifiansyah MR, Setiyowati PAI, *et al*. Antiviral potential of *Alpinia purpurata* against DENV-4: integrated *in vitro* and *in silico* evaluation of non-structural protein inhibition. Nat Eng Sci. 2026.
41. Halim JAN, Halim SN, Denis D, Haryanto S, Dharmana E, Hapsari R, *et al*. Antiviral activities of curcumin and 6-gingerol against infection of four dengue virus serotypes in A549 human cell line *in vitro*. Indones J Biotechnol. 2021;26:41.
42. Kaushik S, Jangra G, Kundu V, Yadav JP, Kaushik S. Anti-viral activity of *Zingiber officinale* (ginger) ingredients against the chikungunya virus. VirusDisease. 2020;31:270–276.

****